The severe acute respiratory syndrome coronavirus 2 (SARS-CoV-2) envelope (E) protein harbors a conserved BH3-like sequence

Vincent Navratil [1,2], Loïc Lionnard [3], Sonia Longhi [4], J. Marie Hardwick [5], Christophe Combet [6] and Abdel Aouacheria [3,*]

[1] PRABI, Rhône Alpes Bioinformatics Center, UCBL, Lyon1, Université de Lyon, Lyon, France.

[2] European Virus Bioinformatics Center, Leutragraben 1, D-07743 Jena, Germany

[3] ISEM, Institut des Sciences de l'Evolution de Montpellier, Université de Montpellier, UMR 5554, CNRS, IRD, EPHE, Place Eugène Bataillon, 34095 Montpellier, France

[4] CNRS and Aix-Marseille Univ, Laboratoire Architecture et Fonction des Macromolecules Biologiques (AFMB), UMR 7257, Marseille, France.

[5] W. Harry Feinstone Department of Molecular Microbiology and Immunology, Johns Hopkins University Bloomberg School of Public Health, Baltimore, Maryland 21205, USA

[6] Centre de Recherche en Cancérologie de Lyon, UMR Inserm U1052, CNRS 5286, Université Claude Bernard Lyon 1, Centre Léon Bérard, Lyon, France.

* Corresponding author

Abdel Aouacheria, ISEM, Institut des Sciences de l'Evolution de Montpellier, Université de Montpellier, CNRS, EPHE, IRD, Montpellier, France. Phone : +33467143751

abdel.aouacheria@umontpellier.fr

Abstract

Following the outbreaks of severe acute respiratory syndrome coronavirus (SARS-CoV) in 2002 and Middle East respiratory syndrome coronavirus (MERS-CoV) in 2012, the novel coronavirus SARS-CoV-2 emerged at the end of 2019. SARS-CoV-2 is a highly infectious pathogen that rapidly spread around the world causing the worst pandemic in the past 100 years. SARS-CoV-2 shares high sequence homology with SARS-CoV and causes coronavirus disease 2019 (COVID-19), leading to pneumonia and severe acute respiratory distress syndrome. Although probably not as lethal as SARS-CoV, its robust transmissibility by asymptomatic individuals is an important contributor to the pandemic.

Like other betacoronaviruses, SARS-CoV-2 encodes four major structural proteins: spike (S), membrane (M), nucleocapsid (N) and envelope (E). SARS-CoV E protein is abundant in infected cells and plays a crucial role in viral particle assembly. Moreover, the E proteins of SARS coronaviruses likely have important roles in pathogenesis by manipulating a number of cellular processes. Thus, SARS-CoV-2 E protein could also be a critical virulence factor. Ectopic expression of SARS-CoV E was reported to trigger apoptotic cell death of T lymphocytes, which could potentially contribute to the lymphopenia observed in fatal cases, though a causal association is unproven. A potential mechanism for inducing apoptosis was reported to involve an interaction between a putative Bcl-2 homology 3 (BH3)-like motif in SARS-CoV E and the anti-apoptotic host protein Bcl-xL. Here we provide the first computational evidence indicating that both the SARS-CoV E and SARS-CoV-2 E have a C-terminal BH3-like motif. We used available sequence data for SARS-CoV-2 and related coronaviruses combined with structural information to evaluate the structure to biological activity relationships of the SARS-CoV-2 E BH3-like motif. Our analysis reveals a predicted interactome for E that is extensively wired to the Bcl-2 apoptotic switch that could potentially be a therapeutic target. Last, network reconstruction identified both the BH3-binding protein Bcl-xL and the autophagy effector Beclin 1, another BH3-containing protein, as vulnerable nodes in the host cellular defense system against SARS-CoV-2.

Keywords: coronavirus; covid-19; apoptosis; Bcl-2 family; BH3 motifs; protein-protein interactions; structure-function relationships; virus-host interactions

1. Introduction

A novel virus of the *Coronaviridae* family, designated as severe acute respiratory syndrome coronavirus 2 (SARS-CoV-2), has been identified as the causative agent of coronavirus disease 2019 (COVID-19) (*1*). While its exact origins are still debated (*2-4*), it is known that SARS-CoV-2 belongs to the β genus (subgenus: *Sarbecovirus*) of the order Nidovirales, subfamily *Orthocoronavirinae*. Coronaviruses of this subfamily generally encode four major structural proteins in their genomes: spike (S), membrane (M), nucleocapsid (N) and envelope (E) (*3-6*). The E protein of the related SARS disease virus (SARS-CoV) has been implicated in pathogenesis and in modulation of apoptosis

and other host responses, but much less is known about the E protein in SARS-CoV-2 (*7, 8*).

The CoV E protein is the smallest of the virion structural proteins, consisting of only 75-109 amino acids across coronaviruses (for a recent review, see (*9*)). Recent biochemical and structural data revealed that SARS-CoV E is a viroporin endowed with ion channel and membrane-permeabilizing activities (*10*), forming homopentameric transmembrane α-helical bundles in lipid bilayers (*11*). This protein is abundant in infected cells where it plays a crucial role in virus particle assembly, and appears to have multiple effects on membranes (*12-14*). Compared to *wild-type* controls, recombinant coronaviruses lacking the E gene have significantly lower viral titers and reduced virus maturation and propagation (*15-17*). E-deficient SARS-CoV is also severely attenuated *in vivo*, exhibiting diminished pathogenic effects (*7, 18*) and inability to replicate in the central nervous system (*7*), suggesting that the E protein may act as an important virulence factor in coronaviruses.

One potential virulence mechanism of the SARS-CoV E protein is via a sequence motif at its extreme C-terminus reported to bind to PSD95/DLG1/ZO-1 (PDZ) domains in other proteins (*19*). This PDZ-binding motif (PBM) in SARS-CoV E is one of many types of small amino acid sequence elements that mediate protein-protein interactions (PPI), and are collectively referred to as short linear motifs (SLiMs). Like many other SLiMs, the PBM found in SARS-CoV E is present at the C-terminus within an intrinsically disordered region (*20*). Through its PBM, SARS-CoV E was shown to engage in interactions with the globular PDZ domains of multiple host proteins such as syntenin and PALS1, and these latter interactions may contribute to airway inflammation and permeability of the lung epithelial barrier (*18, 19*). Several interesting host proteins were recently reported to bind the E protein of COVID-19 virus SARS-CoV-2 using mass-spec pull-down, including bromodomain proteins involved in immune responses and targeted by other viruses (*21*). Several other host factors identified in this study suggest additional potential roles for E in manipulating host cell transcription and the Golgi vesicle trafficking pathway (*21*). SARS-CoV-2 E pulled down a subunit of the Golgi adaptor complex AP-3 that is targeted by HIV and West Nile virus (*22, 23*).

Another potential virulence mechanism of the SARS virus E protein is via a second type of SLiM motif resembling the Bcl-2 homology 3 (BH3) motif found in pro-apoptotic BCL2 family proteins (*8*). This BH3-like motif was reported to encompass residues 51 to 58 (LVKPTVYV) in the C-terminal region of SARS-CoV E, and subsequent mutagenesis

experiments revealed that this amino acid stretch was important for interaction with Bcl-xL (*8*). Consistent with a functional BH3 motif in the E protein, ectopic expression of SARS-CoV E induced apoptosis in T-cells, which was inhibited by the prosurvival Bcl-2 family member Bcl-xL (BCL2L1) (*8*). Although this finding contrasts with in vivo studies of the avirulent E-deficient SARS-CoV, a unifying hypothesis would be if SARS-CoV E suppresses host cell stress responses, as suggested, leading to increased cell death and suppression of beneficial immune responses (*14*). Alternatively, E could activate a harmful overzealous immune response. However, follow-up studies are needed, as each of these molecular interactions is supported primarily by a single report.

BH3 motifs form a newly defined class of SLiMs (*24*) that have well-studied roles in the apoptotic PPI network, by binding to globular proteins of the Bcl-2 family (*25, 26*). BH3 motifs were described or predicted in proteins from eukaryotes (primarily mammals) and from several unrelated microbial species: DNA viruses (HHV8, HBV, HCV), RNA viruses (e..g. Newcastle disease virus) and bacteria (*Photorhabdus luminescens*). The evolution of BH3 motifs appears to involve processes of divergent evolution, transfer events and random/convergent evolution (*24*), including possibly through viral mimicry as previously suggested for other SLiMs (*27, 28*). Elaborating on previous works (*24, 29*), we provide here the first observation that the C-terminal region of SARS-CoV-2 E also possesses this BH3-like sequence. While great attention has been paid to the role of BH3 motifs in cancer (*30-32*), research efforts are warranted to determine biological, clinical and therapeutic relevance of modulating CoV E BH3-like motifs and their associated PPI networks in the context of coronavirus pathogenesis. The prophylactic interest of using SARS-CoV-2 vaccines with an E protein harboring a mutated or deleted BH3-like motif can now also be explored.

2. Results and Discussion

The BH3-like motif identified by Yang et al. (*8*) in the SARS-CoV E sequence (GenBank Acc.# AAP73416) appears to slightly diverge from the BH3 motif of classical BH3-only proteins, justifying inclusion of SARS-CoV E in a large category of other reported BH3-containing proteins (*29*). This sequence divergence is not surprising given that, like many other well-established SLiMs, BH3 motifs display significant degeneracy, with diverse lengths (7-15 amino acids) and variable sequences at most of their amino acid positions. This is especially evident when structurally and evolutionarily distant BH3-containing proteins are considered altogether in a multiple sequence alignment (*24*) (Fig. 1).

Moreover, viral mimics often bear distant resemblance to host SLiMs (*27, 28*). We used the CoV E sequence (GenBank Acc.# AAP73416) from SARS coronavirus ZJ01 as a reference to determine which viral proteins are most related. The overall sequence similarities between this reference SARS-CoV E protein and the E proteins from human coronavirus Middle East respiratory syndrome (MERS-CoV), CoV-HKU1, CoV-OC43 and CoV-4408 are 69,5%, 68,3%, 67,8 and 65,5%, respectively. In comparison, the percent sequence identity between SARS-CoV E sequence and SARS-CoV-2 E is about 95% (pairwise similarity being 98,7%), reflecting the close genetic proximity between the virus causing the current outbreak and the SARS virus from 2003.

To gain insight into the conservation and evolution of CoV E BH3-like sequences, we performed multiple sequence alignments of CoV E sequences starting with the closest relatives to the SARS-CoV ZJ01 reference sequence in terms of phylogenetic proximity (betacoronaviruses) (Fig. 2) and adding more dissimilar sequences from the three other genera of *Orthocoronavirinae* (alpha-, gamma- and deltacoronaviruses). CoV E protein sequences were found in all clades but with various levels of similarity in the C-terminal domain where the BH3-like motif occurs (Fig. 3). Based on the amino acid sequences of the BH3-like region, we analyzed the phylogenetic relationships between the CoV E proteins from the new SARS-CoV-2 and other coronaviruses derived from various species (Fig. 4). CoV E sequences from gammacoronavirus rooted the phylogenetic tree, which provides evidence that their BH3-like region is more distantly related to the reference ZJ01 sequence than the homologous region from alpha- and deltacoronaviruses. Deltacoronavirus sequences were found to be more akin to sequences from betacoronaviruses than alphacoronavirus sequences. The SARS-CoV-2 E protein is in a cluster with bat CoV isolate RaTG13 and pangolin CoV isolate Guangdong, within a group (100% bootstrap support) comprising the reference ZJ01 sequence, other bat-SARS-like coronaviruses and isolate 007/2004 derived from civet. This result has been initially viewed as being indicative of coronavirus crossing of the animal-human species barrier (*3, 4, 33*), with bats as reservoir hosts and pangolins as intermediate hosts facilitating SARS-CoV-2 transfer to humans, although sampling bias (i.e., under coverage of coronavirus diversity in other species) obscures this interpretation until more data are available (*2*). However, sequences from other human zoonotic coronaviruses (human CoV OC43, 4408, HKU1 and MERS) fell into distinct phylogenetic clades with high probability values.

Motif-based sequence analysis suggested that coronaviruses have evolved a conserved and specific BH3-like motif (Supplementary File S1). Instead of conforming to the 6-mer L^1-X^2-X^3-X^4-X^5-D^6 core pattern (with conserved leucine and aspartic acid residues) characteristic of most BH3 sequences (*24, 29*), the BH3 signature inferred from betacoronavirus E sequences is an atypical 9-mer with a conserved Pro and reads as L^1-X^2-X^3-P^4-X^5-ϕ^6-Ω^7-ϕ^8-Ω^9 (with ϕ indicating a preference for aliphatic residues and Ω for aromatic residues) (Fig. 2, *bottom*). Pro54 is totally conserved and one study found that it is critical for targeting of SARS-CoV E protein to the Golgi (*34*). Mutagenesis of positions Leu51, Val56 and Val58 in the BH3 was reported to abrogate the ability of SARS-CoV E to interact with Bcl-xL (*8*). The influence of the other residues present in the CoV E BH3-like motifs (including the highly conserved Asn48 located three residues upstream of Leu51) on protein stability, subcellular targeting, function and interaction is unknown and awaits further characterization.

To predict structure-activity relationship, we constructed a structural model of the new virus SARS-CoV-2 E guided by the homologous structure of SARS-CoV E (PDB code: 5X29) (*11*). In both the experimental structure for SARS-CoV E (Fig. 5A) and the derived structural model for SARS-CoV-2 E (Fig. 5B), the position of Leu51 is in a loop between two helices whereas the highly conserved Pro54 residue is located at the beginning of the C-terminal α-helix. Thus, despite a proline at this position, the BH3-like motif of SARS-CoV and SARS-CoV-2 E has intrinsic propensity for helix formation, like classical BH3s. Note that only four positions are different between full-length SARS-CoV E and SARS-CoV-2 E: two within the BH3-like helix (Thr55 and Val56 in SARS-CoV E, Ser55 and Phe56 in SARS-CoV-2) and two in a site immediately N-terminal to the PBM (where a pair of residues formed by Glu69 and Gly70 in SARS-CoV E is found instead of a single Arg69 residue in SARS-CoV-2 E). Except for Tyr57 (which contacts Leu28 located in the TM segment of the following chain), the BH3-like region (in red) appears to be only marginally involved in the inter-chain interactions needed to form the protein homo-pentamer (*11*), implying alternative roles for the BH3-like motif. Rather, the external orientation, and extended (i.e. irregular) structure of the BH3-like regions in the homo-pentamer (*35*) makes the CoV E BH3-like segment highly prone to serve as a small binding interface able to engage in transient interactions with protein partners, consistent with being a SLiM (*24*). It is possible that the loop containing Leu51 may adopt a regular secondary structure upon binding to targets to form an extended α-helix, with the conserved Pro54 inducing formation of a kinked π-helix.

Annotation of SARS-CoV-2 E from 3,449 SARS-CoV-2 genomes deposited in GISAID EpiCoV identified changes in at least 10 different residues in the E protein from SARS-CoV-2 isolates (Fig. 5C). Five of these are in regions reported to interact with host proteins, including two in/near the BH3, V58L implicated in binding BCLxL and S50G immediately adjacent, and three in the proximal 4-residue PBM, which would be expected to disrupt binding to PDZ domains (*11*). When these 10 substitutions were mapped onto the SARS-CoV-2 E structural model, we found that the mutated residues are predicted to be primarily solvent-exposed on the pentamer and not buried, or involved in intra- and intermonomer contacts (Fig. 5B, white type). This is in line with previous observations that the hydrophobic core of proteins from RNA viruses shows greater conservation than functional sites on the protein surface (*36, 37*). Interestingly, we also annotated a sequence that harbors a deletion spanning eight amino acids (including a conserved Cys residue) occurring in a turn present upstream of the BH3-like region (white ribbon in Fig. 5B, red box in 5C). In addition to shortening the transmembrane domain, which may affect subcellular localization (e.g. by enhancing retention in the Golgi (*38*)), this deletion could potentially interfere with the binding properties of the SARS-CoV-2 E BH3-like motif by introducing local conformational rearrangements.

Last, our analysis of the SARS-CoV-2 interactome using the VirHostNet 2.0 interology webservice (*39*) (Fig. 6) revealed that the predicted SARS-CoV-2 network appears to be wired to the Bcl-2 apoptotic switch by the nonstructural protein NS7a and by protein E. Interestingly, in this interactome, NS7a contacts the five major anti-apoptotic Bcl-2 proteins (Bcl-xL/BCL2L1, BCL2, BCL-w/BCL2L2, MCL-1 and Bfl-1/BCL2A1) (*40*), suggesting that this protein might act as a universal modulator of prosurvival Bcl-2 family proteins during infection. Because many viruses have evolved strategies to interfere with apoptosis (*41*), experimental evidence is needed to establish if the E protein from SARS-CoV-2 directly or indirectly targets prosurvival Bcl-2 homologs to modulate cell viability. Contradictory results have been reported regarding CoV E ability to induce or repress apoptosis (*8, 42, 43*). Overexpressed epitope-tagged SARS-CoV E was found to promote apoptotic cell death in the Jurkat T cell line (*8*), similar to 17Cl-1 cells infected with the mouse hepatitis virus (MHV) (murine coronavirus) (*42*). Interestingly, although apoptosis of SARS-CoV-2-infected T cells has not yet been established (*44*), lymphocytopenia seems to be a common feature of COVID-19 patients (*45*). In contrast, cells infected by a coronavirus lacking E (SARS-CoV∆E) were more primed for apoptosis than those infected with the *wt* strain (*43*). This latter study also suggested that CoV E

may have an anti-apoptotic function by suppressing the unfolded protein response (UPR), likely as a survival mechanism important for virus dissemination (*46*). It may well be that CoV E activity could protect cells from cell death at early stages post-infection by regulating the UPR, and induce apoptosis at a later stage via Bcl-xL sequestration at the Golgi (*8*) or through its viroporin activity (*10, 11*). Yang et al. (*8*) demonstrated that the interaction of SARS-CoV E with Bcl-xL is mediated by the BH3-like region of SARS-CoV E and the BH3 motif of Bcl-xL. Anti-apoptotic Bcl-2 proteins normally accommodate the BH3 motif from typical BH3-only proteins in a hydrophobic receptor cleft partly formed by their own BH3 region (*29-32*). Hence, it remains to be determined whether SARS-CoV-2 E BH3 can bind in the hydrophobic groove of Bcl-xL or at another, distinct interface. It might also be interesting to assess the ability of BH3-mimetics like ABT-737, which tightly binds to the hydrophobic BH3-binding groove of Bcl-xL (*47*), to inhibit binding of SARS-CoV-2 E to Bcl-xL. Bcl-xL and other family members also has other functions involving mitochondria and energetics that could be the targets of viral proteins (*48, 49*).

In our reconstructed cellular interactome (Fig. 7), the SARS-CoV-2 non-structural protein NS7a and protein E are linked to Beclin 1 (BECN1), which also harbors a BH3-like motif (Fig. 1) (*50*). Beclin 1 (also known as autophagy-related protein Atg6 or Vps30) is a component of the lipid kinase (PIK3C2/VPS34) complex important for autophagosome formation. Beclin 1 appears to coordinate apoptosis versus autophagy depending on its interacting partners. The BH3 of Beclin 1 interacts with the anti-apoptotic protein Bcl-2 or Bcl-xL, which limits autophagy under basal conditions (*50, 51*). To initiate autophagy following stress, the Bcl-2/Bcl-xL – Beclin 1 interaction is disrupted (*52, 53*). Our predicted SARS-CoV-2 PPI network indicates that Bcl-xL provides a direct link connecting viral proteins to the autophagy regulator Beclin 1 (Fig. 7, yellow lines). Proteins that bridge different molecular functions in interaction networks are often referred to as bottleneck proteins. The fact that Beclin-1 interacts with many protein partners in the host interactome suggests that it is a hub. In PPI networks, hub-bottleneck proteins tend to be essential, often disease-contributing proteins (*54, 55*) that represent preferential targets in virus infections (*56*). Coronaviruses (including SARS-CoV) were recently reported to target Beclin 1 through their papain-like proteases to induce autophagy (*57*), thereby reducing downstream innate immune signalling. If SARS-CoV-2 also exploits the Beclin 1 hub, possibly through Bcl-xL targeting by E consistent with our analysis, this could contribute to pathogenicity by inhibiting antiviral innate immunity and concomitantly facilitate virus replication (*58, 59*). In support to this, molecular actors implicated in autophagy and interferon type I response appear to

aggregate in local interactome neighborhoods (Fig. 7, left) topologically connected to the SARS-CoV-2 network through Bcl-xL (Fig. 7, right). It is tempting to speculate that SARS-CoV-2 may exploit both types of BH3s, cellular and viral (based on linear motif mimicry) (*27, 28, 60*), to modulate host immune responses.

Like SARS-CoV (*61*), SARS-CoV-2 may be able to infect multiple cell types in several organs, with immune cells (in particular T-cells (*44*)) and lung epithelial cells as prominent targets for the novel coronavirus. The SARS-CoV E protein has been reported to interact with the anti-apoptotic Bcl-2 family protein Bcl-xL through a BH3-like motif located in its C-terminal portion. Considering the importance of Bcl-2 homologs and BH3-containing proteins in pathophysiological settings, the relevance of this interaction and its extrapolation from SARS-CoV to the novel coronavirus SARS-CoV-2 may be revealing about the pathogenesis of COVID-19. In particular, detailed structural characterization and the identification of small molecule drugs able to disrupt this interaction could therefore provide a targeted therapeutic approach where coronavirus treatments are currently lacking or reliant on convalescent sera (*62*). Recombinant SARS-CoV-2 deleted or mutated in the BH3-like region of E might also prove valuable for the design of a live, attenuated vaccine, with an E protein sufficiently intact to maintain structural integrity necessary for the virus life cycle, but mutated enough to abolish protein-protein interactions involved in viral pathogenicity. Last, PPI network reconstruction predicted that both the BH3-binding protein Bcl-xL and the BH3-bearing protein Beclin 1 might be (respectively directly and indirectly) targeted by SARS-CoV-2 to its own advantage, i.e., for interference with antiviral innate immune pathways.

3. Methods and materials

3.1. Database mining, sequence alignments and phylogenetic reconstruction

UniProtKB and GenBank nucleotide and protein sequence databases were searched for sequences related to human SARS-CoV E (Supplemental Table S1). Pangolin CoV E nucleic sequence was *de novo* assembled using metaSPADes v3.13.0 (*63*) from PRJNA573298 project raw reads data (*64*) after carefully removing reads mapped on *Manis javanica* genomic sequences (INSDC: JSZB00000000.1) using bwa. Homologous sequences were aligned with the ClustalW alignment program implemented in the graphical multiple sequence alignment editor SeaView (*65*) or at NPS@ (*66*) using BLOSUM alignment matrices followed by manual optimization after visual

inspection. Consensus sequence logos were generated with the online software WebLogo. A phylogenetic tree was calculated on 67 sites, with 1000 bootstrap replicates, using the BIONJ algorithm (*67*) embedded in Seaview v5.0.2.

3.2. Motif-based sequence analysis

A de novo motif discovery approach was implemented that used the MEME Suite (*68*). A MEME formatted motif was generated from a seed FASTA file of representative BH3-like sequences of coronaviruses. MAST was used to search UniProtKB (release 2019_10) for sequences that match the MEME motif. For hit ranking, the P-value and E-value were computed.

3.3. Structural analysis

The SARS-CoV-2 E protein has been modeled using M4T (*69*) and the known 3D structure of SARS-CoV E as template (PDB code: 5X29). The software PyMOL (https://www.pymol.org) was used for preparing the illustrations.

3.4. Interactome analysis

The predicted protein-protein interaction network of SARS-CoV-2 was constructed by using the VirHosNet 2.0 interology web service (*39*) on the COVID-19/SARS-CoV-2 special release (March 2020). We used the SARS-CoV-2 proteins annotated from Uniprot (https://covid-19.uniprot.org/) as a seed and inferred interology using gold standard protein-protein interaction annotated in VirHostNet. Interologs were defined based on known SARS-CoV protein-protein interactions by using 95% percent identity and 95 % protein coverage blastp thresholds. The putative SARS-CoV-2 interactome comprised 114 proteins and 218 protein-protein interactions and was completed with the recent experimental protein-protein interaction dataset published in (*21*). We used VirHosNet 2.0 web service to explore the links between SARS-CoV-2 cellular protein partners and Beclin 1 in the context of autophagy and interferon type I response molecular interaction subnetworks by using a reconstructed cellular protein interactome as we have previously described (*70, 71*).

Acknowledgments

This work was performed using the computing facilities of the LBBE/PRABI-AMSB. We gratefully acknowledge the authors, originating and submitting laboratories of the

sequences from GISAID's EpiCov Database (Acknowledgment Table is Supplementary Table S3).

Conflict of interest: None declared.

Funding

This research was supported by CNRS, Montpellier University and National Institutes of Health USA grant R21 AI144373.

Legend to figures

Figure 1. Alignment of BH3 regions from Bcl-2 family members, classical BH3-only proteins and other BH3-like sequences. Columns left to right indicate accession identifiers, species abbreviations, sequence names and PubMed Identifiers (PMID). Numbers refer to starting and ending positions of each BH3-containing region. The two most conserved Leu and Asp residues are highlighted in red. The additional BH3 sequences reported in human BID-BH3-B, mouse NOXA and human ATR were omitted for the sake of clarity. ANTI: anti-apoptotic; PRO: pro-apoptotic; Act: activator BH3-only protein; Sen: sensitizer BH3-only protein. STRUCT: experimentally determined structured protein; STRUCT (pred): protein predicted to be structured; IDP: protein experimentally shown as being disordered; IDP (pred): protein predicted to be intrinsically disordered; MIX: protein experimentally shown to contain both disordered and structured regions. MIX (pred): protein predicted to contain both disordered and structured regions. Residue conservation is indicated in shades of colors (darker represents higher degree of conservation). Fixed amino acid positions can hardly be identified in BH3 and BH3-like sequences, and even the typical Leu and Asp residues are not universally conserved among all BH3-bearing proteins. Thus, structural determinations of complexes between BH3 peptides (or BH3-containing proteins) and Bcl-2 homologous proteins and experimental (biochemical and/or cell-based) evidence for direct interactions between them are critical additional criteria to validate BH3 motifs, in addition to sequence-based inference (*29*). Note that the BH3 motif is an unusual SLiM type as it is found both in structured proteins, including Bcl-2 homologs, and in intrinsically disordered proteins (IDPs), such as classical BH3-only proteins (*24*). The figure was adapted from (*24*). Species abbreviations are as follows: Hs, *Homo sapiens;* Mm, *Mus musculus;* Dm, *Drosophila melanogaster;* Hv, *Hydra vulgaris;* Lb, *Lubomirskia*

baikalensis; Aq, *Amphimedon queenslandica;* Am, *Ambystoma mexicanum;* Ce, *Caenorhabditis elegans;* Pl *Photorhabdus luminescens;* NDV, *Newcastle disease virus;* HHV8*, Human herpesvirus 8 (Kaposi's sarcoma-associated herpesvirus);* HBV, *Hepatitis B Virus;* HCV, *Hepatitis C Virus;* Sc, *Saccharomyces cerevisiae;* Sp, *Schizosaccharomyces pombe;* SARS: *human SARS-CoV;* SARS2: *human SARS-CoV-2.* Viral entries were italicized.

Figure 2. Alignment of BH3-like motifs in betacoronavirus E proteins. The CoV E protein (75 amino-acid long) consists of three domains: (i) the amino (N)-terminal domain; (ii) the transmembrane domain (TMD); (iii) and the carboxy (C)-terminal domain. The C-terminal domain comprises a BH3-like motif and a PDZ-binding motif (PBM) at its extremity. The conserved Leu and Pro residues are highlighted in red. Red dots indicate human coronaviruses. Bottom logo map reflects amino acid prevalences.

Figure 3. Sequence alignment of the BH3-like region of CoV E proteins from other non-betacoronaviruses. The CoV E protein sequences of selected alpha-, gamma- and deltacoronavirus were aligned. The region encompassing the BH3-like region of the human SARS-CoV ZJ01 served as the reference sequence. The conserved Leu and Pro residues are highlighted in red. Red dots: human coronaviruses. Bottom logo map reflects amino acid prevalences.

Figure 4. Phylogenetic tree of CoV E proteins from SARS-CoV-2 and other representative coronaviruses. Red dots indicate human viruses. SARS-CoV-2 sequences are in white. The tree was calculated using the BioNJ method on the C-terminal domain of CoV E proteins encompassing the BH3-like motif (or homologous site). Numbers indicate bootstrap percentages after 1000 replications; values below 50% are not reported. Branch lengths are proportional to distances between sequences.

Figure 5. Structural analysis of SARS-CoV and SARS-CoV-2 E proteins.

(A) Experimentally determined NMR structure of the SARS-CoV E protein pentamer (PDB code: 5X29). The five chains (C1 to C5) were colored as follows: C1 (green), C2 (yellow), C3 (dark green), C4 (yellow) and C5 (dark green). Residues from the BH3-like core segment (LVKPTVYVY) are shown in red. The positions of the conserved Leu51 (blue) and Pro54 (cyan) residues are indicated. Interchain contacts between monomers are indicated, Leu28 (green or yellow spheres) on one chain and Tyr57 (red spheres) in the following chain. Note that the recombinant SARS-CoV-2 E protein used to generate the 5X29 structure lacked ten residues at the C-terminus. (B) Homology-driven model of

the SARS-CoV-2 E protein based on 5X29. Only one chain (framed in (A)) is shown. Deleted amino acids from the EPI_ISL_41375225865_26065 translated sequence (see panel C) are colored in white. Other detected point mutations are indicated (they were also reported as white dots in panel A, bottom). The indicated PBM mutations and as well as the mutation affecting Ser6 are out of view. (C) Sequence alignment between SARS-CoV-2 E reference sequence and translated short reads from coronavirus genomes. Except for the reference human SARS-CoV-2 E sequence (GenBank accession number YP_0097243921), other sequences with EPI-ISL-* accession numbers (Supplemental Table S2) were retrieved from GISAID (https://www.gisaid.org/) (*72*) and annotated using tblastn. Residues that differ from the reference SARS-CoV-2 E sequence are highlighted in red. The deletion of eight residues detected in one putative SARS-CoV-2 E sequence is framed. Asterisks in the consensus line indicate positions that are fully conserved. Colons indicate positions that have strongly similar residues and dots are assigned to weakly similar positions.

Figure 6. SARS-CoV-2:human predicted interactome.

SARS-CoV-2/human interologs are anchored on the known SARS-CoV/human protein-protein interaction network. Each node corresponds to a pair of homologous proteins: a SARS-CoV homolog (red node) and a human host protein (blue node). Node size is proportional to the number of cellular partners in the infected cell. Each edge in the interolog network represents an interaction conserved in both species (interolog). The predicted protein-protein interaction between SARS-CoV-2 E (VEMP_CVHSA) and BCL2L1 (BCL2L1_HUMAN) is highlighted in yellow. Nodes that represent anti-apoptotic Bcl-2 family members are colored in green.

Figure 7: Network links between SARS-CoV-2 proteins, Bcl-xL and Beclin 1.

Left: Connection between the SARS-Cov-2 interactome and proteins involved in autophagy and interferon type I response. The autophagy and interferon type I response are contextualized in the graph as a molecular interaction subnetwork by using the human interactome as a framework. Each node corresponds to a protein and each edge to an interaction. Right: zoomed-in image of the framed part. The protein-protein interactions between SARS-CoV-2 E (VEMP_CVHSA) and Bcl-xL (BCL2L1_HUMAN), SARS-CoV-2 NS7a and Bcl-xL (BCL2L1_HUMAN), and Bcl-xL (BCL2L1_HUMAN) and Beclin 1 (BECN1_HUMAN) are highlighted in yellow.

Supplementary data

Supplementary File S1: Output file from the MEME-MAST analysis. The results show the sequences with significant overall matches to the query motif derived from the alignment of representative BH3-like sequences of coronaviruses.

Supplemental Table S1: Dataset used in this study including Accession numbers, taxonomy and protein information (amino acid sequence, length).

Supplementary Table S2: Information on SARS-CoV-2 isolates from different patients whose sequence was used in this study.

Supplementary Table S3: GISAID Acknowledgment table

References

1. N. Zhu *et al.*, A Novel Coronavirus from Patients with Pneumonia in China, 2019. *The New England journal of medicine* **382**, 727-733 (2020).
2. K. G. Andersen, A. Rambaut, W. I. Lipkin, E. C. Holmes, R. F. Garry, The proximal origin of SARS-CoV-2. *Nature medicine*, (2020).
3. P. Zhou *et al.*, A pneumonia outbreak associated with a new coronavirus of probable bat origin. *Nature* **579**, 270-273 (2020).
4. F. Wu *et al.*, A new coronavirus associated with human respiratory disease in China. *Nature* **579**, 265-269 (2020).
5. C. A. de Haan, P. J. Rottier, Molecular interactions in the assembly of coronaviruses. *Adv Virus Res* **64**, 165-230 (2005).
6. P. S. Masters, The molecular biology of coronaviruses. *Adv Virus Res* **66**, 193-292 (2006).
7. M. L. Dediego *et al.*, Pathogenicity of severe acute respiratory coronavirus deletion mutants in hACE-2 transgenic mice. *Virology* **376**, 379-389 (2008).
8. Y. Yang *et al.*, Bcl-xL inhibits T-cell apoptosis induced by expression of SARS coronavirus E protein in the absence of growth factors. *The Biochemical journal* **392**, 135-143 (2005).
9. D. Schoeman, B. C. Fielding, Coronavirus envelope protein: current knowledge. *Virology journal* **16**, 69 (2019).
10. L. Wilson, C. McKinlay, P. Gage, G. Ewart, SARS coronavirus E protein forms cation-selective ion channels. *Virology* **330**, 322-331 (2004).
11. W. Surya, Y. Li, J. Torres, Structural model of the SARS coronavirus E channel in LMPG micelles. *Biochim Biophys Acta Biomembr* **1860**, 1309-1317 (2018).
12. D. X. Liu, Q. Yuan, Y. Liao, Coronavirus envelope protein: a small membrane protein with multiple functions. *Cellular and molecular life sciences : CMLS* **64**, 2043-2048 (2007).
13. H. Vennema *et al.*, Nucleocapsid-independent assembly of coronavirus-like particles by co-expression of viral envelope protein genes. *The EMBO journal* **15**, 2020-2028 (1996).

14. T. R. Ruch, C. E. Machamer, The coronavirus E protein: assembly and beyond. *Viruses* **4**, 363-382 (2012).
15. J. Ortego, J. E. Ceriani, C. Patino, J. Plana, L. Enjuanes, Absence of E protein arrests transmissible gastroenteritis coronavirus maturation in the secretory pathway. *Virology* **368**, 296-308 (2007).
16. K. M. Curtis, B. Yount, R. S. Baric, Heterologous gene expression from transmissible gastroenteritis virus replicon particles. *Journal of virology* **76**, 1422-1434 (2002).
17. J. Ortego, D. Escors, H. Laude, L. Enjuanes, Generation of a replication-competent, propagation-deficient virus vector based on the transmissible gastroenteritis coronavirus genome. *Journal of virology* **76**, 11518-11529 (2002).
18. J. M. Jimenez-Guardeno *et al.*, The PDZ-binding motif of severe acute respiratory syndrome coronavirus envelope protein is a determinant of viral pathogenesis. *PLoS pathogens* **10**, e1004320 (2014).
19. K. T. Teoh *et al.*, The SARS coronavirus E protein interacts with PALS1 and alters tight junction formation and epithelial morphogenesis. *Molecular biology of the cell* **21**, 3838-3852 (2010).
20. K. Luck, S. Charbonnier, G. Trave, The emerging contribution of sequence context to the specificity of protein interactions mediated by PDZ domains. *FEBS letters* **586**, 2648-2661 (2012).
21. D. E. Gordon *et al.*, A SARS-CoV-2-Human Protein-Protein Interaction Map Reveals Drug Targets and Potential Drug-Repurposing. *bioRxiv*, 2020.2003.2022.002386 (2020).
22. L. Liu *et al.*, Defective HIV-1 particle assembly in AP-3-deficient cells derived from patients with Hermansky-Pudlak syndrome type 2. *Journal of virology* **86**, 11242-11253 (2012).
23. M. Li *et al.*, Identification of antiviral roles for the exon-junction complex and nonsense-mediated decay in flaviviral infection. *Nat Microbiol* **4**, 985-995 (2019).
24. A. Aouacheria, C. Combet, P. Tompa, J. M. Hardwick, Redefining the BH3 Death Domain as a 'Short Linear Motif'. *Trends in biochemical sciences* **40**, 736-748 (2015).
25. M. Kvansakul, M. G. Hinds, The structural biology of BH3-only proteins. *Methods in enzymology* **544**, 49-74 (2014).
26. J. A. Glab, G. W. Mbogo, H. Puthalakath, BH3-Only Proteins in Health and Disease. *Int Rev Cell Mol Biol* **328**, 163-196 (2017).
27. L. B. Chemes, G. de Prat-Gay, I. E. Sanchez, Convergent evolution and mimicry of protein linear motifs in host-pathogen interactions. *Current opinion in structural biology* **32**, 91-101 (2015).
28. P. Hraber *et al.*, Resources to Discover and Use Short Linear Motifs in Viral Proteins. *Trends in biotechnology* **38**, 113-127 (2020).
29. A. Aouacheria, V. Rech de Laval, C. Combet, J. M. Hardwick, Evolution of Bcl-2 homology motifs: homology versus homoplasy. *Trends in cell biology* **23**, 103-111 (2013).
30. S. Cory, A. W. Roberts, P. M. Colman, J. M. Adams, Targeting BCL-2-like Proteins to Kill Cancer Cells. *Trends Cancer* **2**, 443-460 (2016).
31. J. D. Huska, H. M. Lamb, J. M. Hardwick, Overview of BCL-2 Family Proteins and Therapeutic Potentials. *Methods Mol Biol* **1877**, 1-21 (2019).
32. J. Montero, A. Letai, Why do BCL-2 inhibitors work and where should we use them in the clinic? *Cell death and differentiation* **25**, 56-64 (2018).
33. T. T. Lam *et al.*, Identifying SARS-CoV-2 related coronaviruses in Malayan pangolins. *Nature*, (2020).
34. J. R. Cohen, L. D. Lin, C. E. Machamer, Identification of a Golgi complex-targeting signal in the cytoplasmic tail of the severe acute respiratory syndrome coronavirus envelope protein. *Journal of virology* **85**, 5794-5803 (2011).
35. Y. Li, W. Surya, S. Claudine, J. Torres, Structure of a conserved Golgi complex-targeting signal in coronavirus envelope proteins. *The Journal of biological chemistry* **289**, 12535-12549 (2014).

36. S. Warren, X. F. Wan, G. Conant, D. Korkin, Extreme evolutionary conservation of functionally important regions in H1N1 influenza proteome. *PloS one* **8**, e81027 (2013).
37. S. Cheng, C. L. Brooks, 3rd, Viral capsid proteins are segregated in structural fold space. *PLoS computational biology* **9**, e1002905 (2013).
38. S. Munro, An investigation of the role of transmembrane domains in Golgi protein retention. *The EMBO journal* **14**, 4695-4704 (1995).
39. T. Guirimand, S. Delmotte, V. Navratil, VirHostNet 2.0: surfing on the web of virus/host molecular interactions data. *Nucleic acids research* **43**, D583-587 (2015).
40. Y. X. Tan *et al.*, Induction of apoptosis by the severe acute respiratory syndrome coronavirus 7a protein is dependent on its interaction with the Bcl-XL protein. *Journal of virology* **81**, 6346-6355 (2007).
41. J. M. Hardwick, Viral interference with apoptosis. *Semin Cell Dev Biol* **9**, 339-349 (1998).
42. S. An, C. J. Chen, X. Yu, J. L. Leibowitz, S. Makino, Induction of apoptosis in murine coronavirus-infected cultured cells and demonstration of E protein as an apoptosis inducer. *Journal of virology* **73**, 7853-7859 (1999).
43. M. L. DeDiego *et al.*, Severe acute respiratory syndrome coronavirus envelope protein regulates cell stress response and apoptosis. *PLoS pathogens* **7**, e1002315 (2011).
44. X. Wang *et al.*, SARS-CoV-2 infects T lymphocytes through its spike protein-mediated membrane fusion. *Cell Mol Immunol*, (2020).
45. M. Zheng *et al.*, Functional exhaustion of antiviral lymphocytes in COVID-19 patients. *Cell Mol Immunol*, (2020).
46. S. Li, L. Kong, X. Yu, The expanding roles of endoplasmic reticulum stress in virus replication and pathogenesis. *Critical reviews in microbiology* **41**, 150-164 (2015).
47. T. Oltersdorf *et al.*, An inhibitor of Bcl-2 family proteins induces regression of solid tumours. *Nature* **435**, 677-681 (2005).
48. J. M. Hardwick, Y. B. Chen, E. A. Jonas, Multipolar functions of BCL-2 proteins link energetics to apoptosis. *Trends in cell biology* **22**, 318-328 (2012).
49. E. A. Jonas, G. A. Porter, K. N. Alavian, Bcl-xL in neuroprotection and plasticity. *Front Physiol* **5**, 355 (2014).
50. S. Sinha, B. Levine, The autophagy effector Beclin 1: a novel BH3-only protein. *Oncogene* **27 Suppl 1**, S137-148 (2008).
51. R. Kang, H. J. Zeh, M. T. Lotze, D. Tang, The Beclin 1 network regulates autophagy and apoptosis. *Cell death and differentiation* **18**, 571-580 (2011).
52. J. P. Decuypere, J. B. Parys, G. Bultynck, Regulation of the autophagic bcl-2/beclin 1 interaction. *Cells* **1**, 284-312 (2012).
53. W. C. Chiang *et al.*, High-Throughput Screens To Identify Autophagy Inducers That Function by Disrupting Beclin 1/Bcl-2 Binding. *ACS chemical biology* **13**, 2247-2260 (2018).
54. V. Navratil, B. de Chassey, C. R. Combe, V. Lotteau, When the human viral infectome and diseasome networks collide: towards a systems biology platform for the aetiology of human diseases. *BMC systems biology* **5**, 13 (2011).
55. A. L. Barabasi, N. Gulbahce, J. Loscalzo, Network medicine: a network-based approach to human disease. *Nature reviews. Genetics* **12**, 56-68 (2011).
56. L. L. Zheng *et al.*, The domain landscape of virus-host interactomes. *BioMed research international* **2014**, 867235 (2014).
57. X. Chen *et al.*, Coronavirus membrane-associated papain-like proteases induce autophagy through interacting with Beclin1 to negatively regulate antiviral innate immunity. *Protein & cell* **5**, 912-927 (2014).
58. Y. Tian, M. L. Wang, J. Zhao, Crosstalk between Autophagy and Type I Interferon Responses in Innate Antiviral Immunity. *Viruses* **11**, (2019).
59. E. V. Mesev, R. A. LeDesma, A. Ploss, Decoding type I and III interferon signalling during viral infection. *Nat Microbiol* **4**, 914-924 (2019).

60. E. Guven-Maiorov, C. J. Tsai, R. Nussinov, Pathogen mimicry of host protein-protein interfaces modulates immunity. *Semin Cell Dev Biol* **58**, 136-145 (2016).
61. J. Gu *et al.*, Multiple organ infection and the pathogenesis of SARS. *The Journal of experimental medicine* **202**, 415-424 (2005).
62. E. M. Bloch *et al.*, Deployment of convalescent plasma for the prevention and treatment of COVID-19. *The Journal of clinical investigation*, (2020).
63. S. Nurk, D. Meleshko, A. Korobeynikov, P. A. Pevzner, metaSPAdes: a new versatile metagenomic assembler. *Genome research* **27**, 824-834 (2017).
64. P. Liu, W. Chen, J. P. Chen, Viral Metagenomics Revealed Sendai Virus and Coronavirus Infection of Malayan Pangolins (Manis javanica). *Viruses* **11**, (2019).
65. M. Gouy, S. Guindon, O. Gascuel, SeaView version 4: A multiplatform graphical user interface for sequence alignment and phylogenetic tree building. *Molecular biology and evolution* **27**, 221-224 (2010).
66. C. Combet, C. Blanchet, C. Geourjon, G. Deleage, NPS@: network protein sequence analysis. *Trends in biochemical sciences* **25**, 147-150 (2000).
67. O. Gascuel, BIONJ: an improved version of the NJ algorithm based on a simple model of sequence data. *Molecular biology and evolution* **14**, 685-695 (1997).
68. T. L. Bailey *et al.*, MEME SUITE: tools for motif discovery and searching. *Nucleic acids research* **37**, W202-208 (2009).
69. D. Rykunov, E. Steinberger, C. J. Madrid-Aliste, A. Fiser, Improved scoring function for comparative modeling using the M4T method. *J Struct Funct Genomics* **10**, 95-99 (2009).
70. I. P. Gregoire *et al.*, IRGM is a common target of RNA viruses that subvert the autophagy network. *PLoS pathogens* **7**, e1002422 (2011).
71. V. Navratil *et al.*, System-level comparison of protein-protein interactions between viruses and the human type I interferon system network. *J Proteome Res* **9**, 3527-3536 (2010).
72. Y. Shu, J. McCauley, GISAID: Global initiative on sharing all influenza data - from vision to reality. *Euro Surveill* **22**, (2017).

										PMID:	
BCL-2 homologs	P10415	Hs	BCL2	86	LSPVPPVVHLTL-RQAG--DDFSRRYRRDFAEM	115	ANTI	6093263	STRUCT
	Q07817	Hs	BCL2L1	79	EVIPMAAVKQAL-REAG--DEFELRYRRAFSDL	108	ANTI	8358789	STRUCT
	Q92843	Hs	BCL2L2	35	EGPAADPLHQAM-RAAG--DEFETRFRRTFSDL	64	ANTI	8761287	STRUCT
	Q07820	Hs	MCL1	202	SGATSRKALETL-RRVG--DGVQRNHETAFQGM	231	ANTI	7682708	STRUCT
	Q9HD36	Hs	BCL2L10	28	EPAPSTPEAAVL-RSAA--ARLRQIHRSFFSAY	57	ANTI	11593390	STRUCT
	Q16548	Hs	BCL2A1	26	PGSGPSKTSRVL-QNVA--FSVQKEVEKNLKSC	55	ANTI	8345191	STRUCT
	P41958	Ce	CED9	105	LPCGVQPEHEMM-RVMG--TIFEKKHAENFETF	134	ANTI	7907274	STRUCT
	Q8T8Y5	Dm	BUFFY	128	SMGIVRDVFPAV-QVLG--DELERMHPRIYNGV	157	ANTI	10801447	STRUCT (pred)
	Q9V9C8	Dm	DEBCL	135	SSHVVYEVFPAL-NSMG--EELERMHPRVYTNI	164	PRO	10684252	STRUCT (pred)
	Q9UMX3	Hs	BOK	59	VPGRLAEVCAVL-LRLG--DELEMIRPSVYRNV	88	PRO	9535847	STRUCT (pred)
	Q07812	Hs	BAX	52	QDASTKKLSECL-KRIG--DELDSNMELQRMIA	81	PRO	8358790	STRUCT
	Q16611	Hs	BAK1	67	PSSTMGQVGRQL-AIIG--DDINRRYDSEFQTM	96	PRO	7715730	STRUCT
	Q9HB09	Hs	BCL2L12	217	KEAILRRLVALL-EEEA--EVINQKLASDPALR	235	PRO	11401436	STRUCT (pred)
	Q9BXK5	Hs	BCL2L13	93	PANPESSMEDCL-AHLG--EKVSQELKEPLHKA	122	PRO	11262395	STRUCT (pred)
	Q9BZR8	Hs	BCL2L14	205	EEQILAKIVELL-KYSG--DQLERKLKKDKALM	234	PRO	11054413	STRUCT (pred)
	Q5TBC7	Hs	BCL2L15	46	CSFDVAIIAGRL-RMLG--DQFNGELEASAKNV	75	PRO	12700646	STRUCT (pred)
	P55957	Hs	BID (A)	79	QEDIIRNIARHL-AQVG--DSMDRSIPPGLVNG	108	PRO (Act)	8918887	STRUCT
	A7LM80	Hv	BCL2-like	39	LKPPVIEIAKTL-QRVG--DELESANTDFFKNM	68	ND	24065732	STRUCT (pred)
	I1GDG3	Aq	BCL2-like	89	GESNAKAVGRRL-AELG--DEIDSMYSGHFEDI	118	ND	20686567	STRUCT (pred)
	Q1RPT5	Lb	BCL2-like	64	ASSMASEVGRRL-AEFG--DQVDGQFYQEMEEI	93	ND	16569194	STRUCT (pred)
	B7SB93	Am	BCL2-like	35	VNESPSAAACHL-RRVA--DELIEENRQLFDSM	64	ND	Prediction	STRUCT (pred)
Classical BH3-only	O43521	Hs	BIM	141	DMRPEIWIAQEL-RRIG--DEFNAYYARRVFLN	170	PRO (Act)	9430630	IDP
	Q9BXH1	Hs	PUMA	130	EEQWAREIGAQL-RRMA--DDLNAQYERRRQEE	159	PRO (Act)	11572983	IDP
	Q92934	Hs	BAD	103	NLWAAQRYGREL-RRMS--DEFVDSFKKGLPRP	132	PRO (Sen)	7834748	IDP
	Q13323	Hs	BIK	50	CMEGSDALALRL-ACIG--DEMDVSLRAPRLAQ	79	PRO (Sen)	7478623	STRUCT (pred)
	Q96LC9	Hs	BMF	126	QHQAEVQIARKL-QCIA--DQFHRLHVQQHQQN	155	PRO (Sen)	11546872	IDP
	O00198	Hs	HRK	26	RSSAAQLTAARL-KALG--DELHQRTMWRRRAR	55	PRO (Sen)	9130713	IDP
	Q13794	Hs	NOXA	18	PAELEVECATQL-RRFG--DKLNFRQKLLNLIS	47	PRO (Act)	10807576	IDP
	O61667	Ce	EGL1	62	ISSIGYEIGSKL-AAMC--DDFDAQMMSYSAHA	91	PRO	9604928	IDP
Other BH3-containing proteins	P21980	Hs	TG2	193	CLILLDVNPKFL-KNAG-RDCSRRSSPVYVGRV	223	PRO	15485857	STRUCT
	O94817	Hs	ATG12	48	AGDTKKKIDILL-KAVG--DTPIMKTKKWAVER	77	PRO	22152474	STRUCT
	Q99638	Hs	RAD9A	9	NVKVLGKAVHSL-SRIG--DELYLEPLEDGLSL	38	PRO	10620799	STRUCT
	P26306	Sp	SpRAD9	9	NLRDLARIFTNL-SRID--DAVNWEINKNQIEI	38	PRO	10996309	MIX (pred)
	Q9TY06	Hs	CED13	48	SNTVEYNIGRKL-TVMC--DEFDSELMSYKEEK	77	PRO	15605074	STRUCT (pred)
	O14791	Hs	APOL1	147	LKSELEDNIRRL-RALA--DGVQKVHKGTTIAN	176	PRO	18505729	STRUCT (pred)
	Q9BQE5	Hs	APOL2	88	LKRELEDHIRKL-RALA--EEVEQVHRGTTIAN	117	NEUTRAL	24901046	STRUCT (pred)
	Q9BWW8	Hs	APOL6	49	LKEDLKGNIDKL-RALA--DDIDKTHKKFTKAN	69	PRO	15671246	STRUCT (pred)
	Q14457	Hs	BECN1	105	DGGTMENLSRRL-KVTG--DLFDIMSGQTDVDH	134	PRO	17337444	STRUCT (pred)
	Q8VE73	Hs	CUL7	1555	RNLLNCLVVRIL-KAHG--DEGLHVDRLVYLVL	1584	PRO	10652310	STRUCT (pred)
	Q15303	Hs	ERBB4	974	FSRMARDPQRYL-VIQG--DDRMKLPSPNDSKF	1003	PRO	16778220	STRUCT (pred)
	P04626	Hs	ERBB2	1109	LQRYSEDPTVPL-PSET--DGYVAPLTCSPQPE	1138	PRO	18420586	STRUCT (pred)
	Q9Y287	Hs	ITM2B	80	ALQPDDVYYCGI-KYIK--DDVILNEPSADAPA	108	PRO	12082633	STRUCT (pred)
	Q96BY2	Hs	MOAP1	109	FLAGEGMTVGELSRALGH-ENGSLDPEQGMIP-	139	PRO	11060313	STRUCT (pred)
	Q8IZY5	Hs	BRCC2	1	-------MVTLL-PIEG--QEIHFFEILESECV	23	PRO	15069058	STRUCT (pred)
	Q9Y5Z4	Hs	SOUL	151	NQEQLLTLASIL-REDG--KVFDEKVYYTAGYN	180	PRO	19901022	STRUCT (pred)
	Q12981	Hs	BNIP1	103	KIAIDNLEKAEL-LQGG--DLLRQRKTTKESLA	132	PRO	12766483	STRUCT (pred)
	Q12982	Hs	BNIP2	77	SGEIDLDGLDTP-SENS--NEFEWEDDLPKPKT	106	PRO	12766483	STRUCT (pred)
	Q12983	Hs	BNIP3	99	DIERRKEVESIL-KKNS--DWIWDWSSRPENIP	128	PRO	9575197	MIX (pred)
	O60238	Hs	BNIP3L	123	EVVEGEKEVEAL-KKSA--DWVSDWSSRPENIP	152	PRO	12766483	MIX (pred)
	Q09969	Ce	CEBNIP3	118	EQVKYKLVREML-PPGKNTDWIWDWSSRPENTP	149	PRO	11114722	MIX (pred)
	Q7L3V2	Hs	BOP	107	FDGSPWLLDRFL-AQLG--DYMSFHFEHYQDNI	136	PRO	23055042	MIX (pred)
	P10909	Hs	CLU	312	DCSTNNPSQAKL-RREL--DESLQVAERLTRKY	341	PRO	21527247	MIX (pred)
	Q7Z6Z7	Hs	HUWE	1969	PGVMTQEVGQLL-QDMG--DDVYQQYRSLTRQS	1998	PRO	15989957	MIX (pred)
	Q9NZZ3	Hs	CHMP5	156	PELDEDDLEAEL-DALG--DELLADEDSSYLDE	185	PRO	12594175	MIX (pred)
	Q9NRA0	Hs	SPHK2	243	TVSGDGLLHEVL-NGLL--DRPDWEEAVKMPVG	272	PRO	12835323	MIX (pred)
	Q9NQS1	Hs	AVEN	134	ESQRGTDFSVLL-SSAG--DSFSQFRFAEEKEW	162	ANTI	22754595	IDP (pred)
	Q9C0C7	Hs	AMBRA1	1204	SSPQPSTSRGLL-PEAG--QLAERGLSPRTASW	1233	PRO	28215535	MIX (pred)
	Q13535	Hs	ATR	466	DMNQKSILWSAL-KQKA--ESLQISLEYSGLKN	484	ANTI	26387736	STRUCT
	Q14643	Hs	ITPR1	2583	FMVIIIVLNLIF-GVII--DTFADLRSEKQKKE	2637	PRO	26976600	STRUCT (pred)
	P13693	Hs	TPT1	9	SHDEMFSDIYKI-REIA--DGLCLEVEGKMVSR	38	ANTI	26813996	STRUCT
	P57764	Hs	GMDMD	139	LRQPEHKVLQQL-RSRG--DNVYVVTEVLQTQK	168	PRO	31839993	STRUCT
	Q8NB16	Hs	MLKL	158	IEASLRRLEINM-KEIK--ETLRQYLPPKCMQE	187	PRO	31839993	STRUCT
	Q8K459	Mm	PXT1	1	---------MQL-RHIG--DSVNHRVIQEHLAQ	21	PRO	21460186	STRUCT (pred)
	Q0GET0	Mm	BLM-S	84	MQLDFQQFLMKL-EKLT--DIRPIPDKEFVETY	113	PRO	25263558	STRUCT (pred)
	C8ZGL9	Sc	YNL305CP	279	IVNLFLSILRIL-ANSN--DDN----------	297	PRO	21673659	STRUCT (pred)
	Q8KT65	Pl	MCF	904	QAVKDLELKAGL-TSVG--DGFEPRQGSADIHQ	933	PRO	12136122	STRUCT (pred)
	Q9QBF1	*HBV-B*	*P (HBSP)*	14	LDDEAGPLEEEL-PRLA--DEGLNRRVAEDLNL	43	PRO	17049490	STRUCT (pred)
	Q05499	*HBV-F*	*HBX*	109	EEYIKDCVFKDW-EELG--EEIRLKVFVLGGCR	138	PRO	16274670	STRUCT (pred)
	P88946	*HHV8*	*VIRF1*	163	RMLAALRRTRGL-QEIG--KGISQDGHHFLVFR	192	ANTI	22685405	STRUCT
	Q9DLD4	*NDV*	*F0*	81	LDAYNRTLTTLL-TPLG--DSIRRIQESVTTSG	110	PRO	21810274	STRUCT
	Q9WBL3	*NDV*	*M*	16	PSSSLLAFPIVL-QDTG--DGKKQITPQYRIQR	45	PRO	21810274	STRUCT
	Q6X1B6	*NDV*	*L*	2111	EVTILGLRVKDL-NKVG--DVIGLVLRGMVSLE	2140	PRO	21810274	STRUCT (pred)
	Q00269	*HCV*	*CORE*	108	GPTDPRRRSRNL-GKVI--DTLTCGFADLMGYI	137	PRO	19605477	MIX (pred)
	AAP73416	*SARS-CoV E*		40	CAYCCNIVNVSL-VKPT--VYVYSRVKNLNSSE	69	PRO	16048439	MIX
	YP_009724392	*SARS-CoV-2 E*		40	CAYCCNIVNVSL-VKPS--FYVYSRVKNLNSSR	69	ND	ND	MIX (pred)

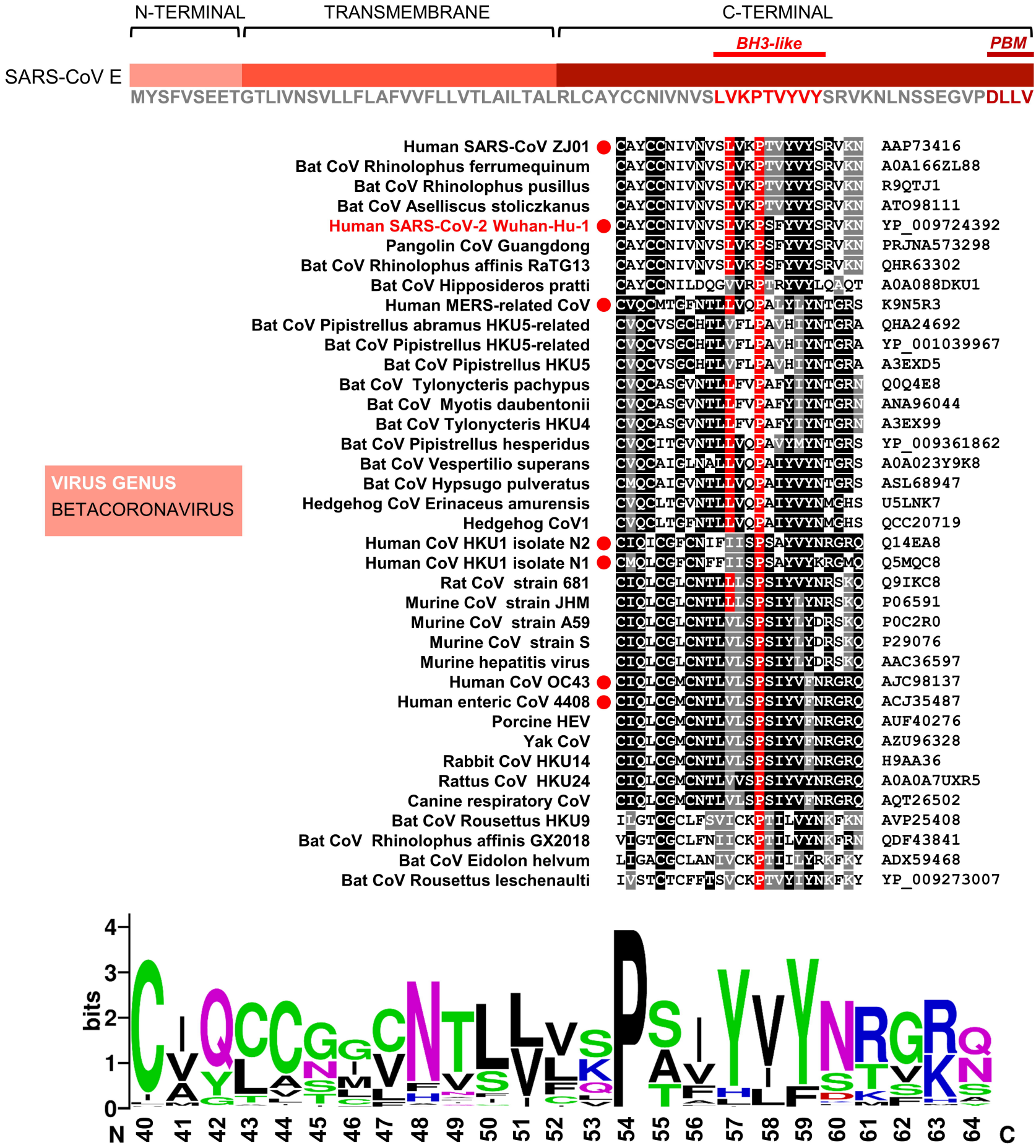
N-TERMINAL
TRANSMEMBRANE
C-TERMINAL
BH3-like
PBM
SARS-CoV E
MYSFVSEETGTLIVNSVLLFLAFVVFLLVTLAILTALRLCAYCCNIVNVSLVKPTVYVYSRVKNLNSSEGVPDLLV
Human SARS-CoV ZJ01 CAYCCNIVNVSLVKPTVYVYSRVKN AAP73416
Bat CoV Rhinolophus ferrumequinum CAYCCNIVNVSLVKPTVYVYSRVKN A0A166ZL88
Bat CoV Rhinolophus pusillus CAYCCNIVNVSLVKPTVYVYSRVKN R9QTJ1
Bat CoV Aselliscus stoliczkanus CAYCCNIVNVSLVKPTVYVYSRVKN ATO98111
Human SARS-CoV-2 Wuhan-Hu-1 CAYCCNIVNVSLVKPSFYVYSRVKN YP_009724392
Pangolin CoV Guangdong CAYCCNIVNVSLVKPSFYVYSRVKN PRJNA573298
Bat CoV Rhinolophus affinis RaTG13 CAYCCNIVNVSLVKPSFYVYSRVKN QHR63302
Bat CoV Hipposideros pratti CAYCCNILDQGVVRPTRYVYLQAQT A0A088DKU1
Human MERS-related CoV CVQCMTGFNTLLVQPALYLYNTGRS K9N5R3
Bat CoV Pipistrellus abramus HKU5-related CVQCVSGCHTLVFLPAVHIYNTGRA QHA24692
Bat CoV Pipistrellus HKU5-related CVQCVSGCHTLVFLPAVHIYNTGRA YP_001039967
Bat CoV Pipistrellus HKU5 CVQCVSGCHTLVFLPAVHIYNTGRA A3EXD5
Bat CoV Tylonycteris pachypus CVQCASGVNTLLFVPAFYIYNTGRN Q0Q4E8
Bat CoV Myotis daubentonii CVQCASGVNTLLFVPAFYIYNTGRN ANA96044
Bat CoV Tylonycteris HKU4 CVQCASGVNTLLFVPAFYIYNTGRN A3EX99
Bat CoV Pipistrellus hesperidus CVQCITGVNTLLVQPAVYMYNTGRS YP_009361862
Bat CoV Vespertilio superans CVQCAIGLNALLVQPAIYVYNTGRS A0A023Y9K8
Bat CoV Hypsugo pulveratus CMQCAIGVNTLLVQPAIYVYNTGRS ASL68947
Hedgehog CoV Erinaceus amurensis CVQCLTGVNTLLVQPAIYVYNMGHS U5LNK7
Hedgehog CoV1 CVQCLTGFNTLLVQPAIYVYNMGHS QCC20719
Human CoV HKU1 isolate N2 CIQICGFCNIFIISPSAYVYNRGRQ Q14EA8
Human CoV HKU1 isolate N1 CMQLCGFCNFFIISPSAYVYKRGMQ Q5MQC8
Rat CoV strain 681 CIQLCGLCNTLLLSPSIYVYNRSKQ Q9IKC8
Murine CoV strain JHM CIQLCGLCNTLLLSPSIYLYNRSKQ P06591
Murine CoV strain A59 CIQLCGLCNTLVLSPSIYLYDRSKQ P0C2R0
Murine CoV strain S CIQLCGLCNTLVLSPSIYLYDRSKQ P29076
Murine hepatitis virus CIQLCGLCNTLVLSPSIYLYDRSKQ AAC36597
Human CoV OC43 CIQLCGMCNTLVLSPSIYVFNRGRQ AJC98137
Human enteric CoV 4408 CIQLCGMCNTLVLSPSIYVFNRGRQ ACJ35487
Porcine HEV CIQLCGMCNTLVLSPSIYVFNRGRQ AUF40276
Yak CoV CIQLCGMCNTLVLSPSIYVFNRGRQ AZU96328
Rabbit CoV HKU14 CIQLCGMCNTLVLSPSIYVFNRGRQ H9AA36
Rattus CoV HKU24 CIQLCGMCNTLVVSPSIYVYNRGRQ A0A0A7UXR5
Canine respiratory CoV CIQLCGMCNTLVLSPSIYVFNRGRQ AQT26502
Bat CoV Rousettus HKU9 ILGTCGCLFSVICKPTILVYNKFKN AVP25408
Bat CoV Rhinolophus affinis GX2018 VIGTCGCLFNIICKPTILVYNKFRN QDF43841
Bat CoV Eidolon helvum LIGACGCLANIVCKPTIILYRKFKY ADX59468
Bat CoV Rousettus leschenaulti IVSTCTCFFTSVCKPTVYIYNKFKY YP_009273007
VIRUS GENUS
BETACORONAVIRUS
bits
0
1
2
3
4
N 40 41 42 43 44 45 46 47 48 49 50 51 52 53 54 55 56 57 58 59 60 61 62 63 64 C

VIRUS GENUS
ALPHACORONAVIRUS

Human CoV NL63 ●	CFTCHYFFSRTLYQPVYKIFLAYQD	QED88021
Human CoV 229E ●	CFTCHMFCNRTVYGPIKNVYHIYQS	QEO75987
Bat CoV Tylonycteris robustula HKU33	CMVCHHLMSGAVYRPVYRVYELYKD	QCX35162
Bat CoV Nyctalus velutinus	CFACHQLMTSAVYKPVHNAYAIYRD	AIA62267
Bat CoV Myotis ricketti	CIACHQFANRTVYSPIYSAYQWYKD	AIA62248
Bat CoV Scotophilus kuhlii GX2018A	CFTCHRLCNNVVYKPVGKVYGVYKS	QDF43791
Bat CoV Scotophilus kuhlii 512r	CFTCHRLCNSVVYRPVGKFYRVYKS	QHA24698
Bat CoV Miniopterus fuliginosus	LFSCHRLCSNTVYRPVYGAYRAYQD	AIA62214
Porcine epidemic diarrhea virus	CFTCHRLCNSAVYTPIGRLYRVYKS	APH81308
Apodemus chevrieri AcCoV-JC34	VGVCCSLTNKVIVLPVKGVYHLYQD	A0A1X9JJV7
Lucheng Rn rat CoV	VGVCCSLTNKVIVLPVKGVYHLYQD	A0A1L7HIW4
Canine CoV strain Insavc-1	CMVCCNLGRTVIIVPARHAYDAYKN	P36696
Feline CoV strain FIPV WSU-79/1146	CMVCCNLGKTIIVLPARHAYDAYKT	Q52PA5
Mink CoV strain WD1133	CMVCCRLSNVVIIAPARQAYNAYKD	D9J205

VIRUS GENUS
GAMMACORONAVIRUS

Avian CoV	ADACCLFWYTWLVIPGVKGTAFVYK	ARJ35794
Turkey CoV	ADACCLFWYTWIVVPGAKGAAFVYN	YP_001941169
Gallus Infectious bronchitis virus	ADACCLFWYTWVVVPGAKGTAFVYK	AYG86350
Duck CoV	VDACCLFWYTWVVVPGAKGTAFVYK	AEO86771
Beluga whale CoV SW1	IDVCLLFCKGWAVDPSVRLVSYAYG	YP_001876438

VIRUS GENUS
DELTACORONAVIRUS

Porcine CoV HKU15	LFYKCYLGAAYLVRPIIVYYSKPNP	YP_009513022
Munia CoV HKU13-3514	LSYKCFLGAKYLVNPIIVYYSKPQT	YP_002308507
Bulbul CoV HKU11-934	LSYKCFLGARYLVNPIIVYYSKPNP	YP_002308480
Thrush CoV HKU12-600	LSYKCFLGARYLVNPIIVYYSKPNP	YP_002308498
White-eye CoV HKU16	LSYKCFLGARYLVNPIIVYYSKPKT	YP_005352839
Sparrow CoV HKU17	LTYKCYLGARYLVNPIIVYYSKPNP	YP_005352847
Magpie-robin CoV HKU18	LSYKCFLGAKYLVNPIIVYYSKPQT	YP_005352855
Common moorhen CoV HKU21	LVYKCYKGATVLLNPFIIFSSKVDP	YP_005352882
Night heron CoV HKU19	FFTRTYTCILHTVKPIYVYLKPAPV	YP_005352864

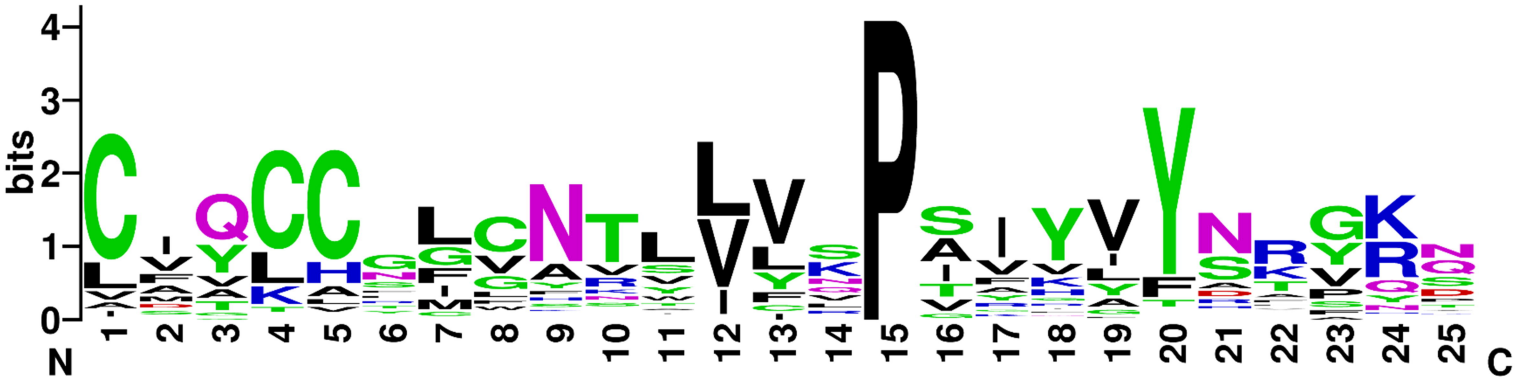

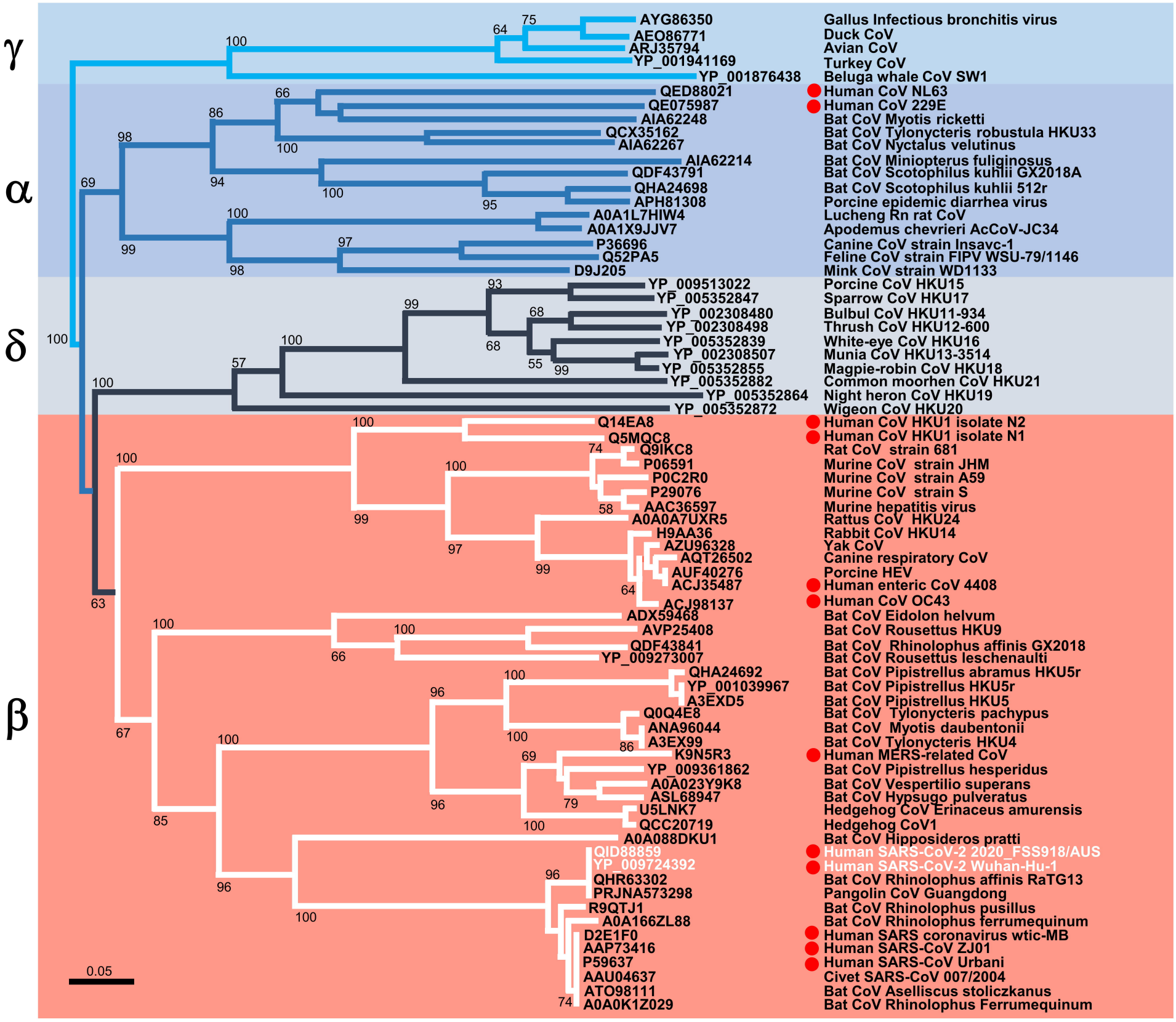
γ
α
δ
β
AYG86350 Gallus Infectious bronchitis virus
AEO86771 Duck CoV
ARJ35794 Avian CoV
YP_001941169 Turkey CoV
YP_001876438 Beluga whale CoV SW1
QED88021 Human CoV NL63
QE075987 Human CoV 229E
AIA62248 Bat CoV Myotis ricketti
QCX35162 Bat CoV Tylonycteris robustula HKU33
AIA62267 Bat CoV Nyctalus velutinus
AIA62214 Bat CoV Miniopterus fuliginosus
QDF43791 Bat CoV Scotophilus kuhlii GX2018A
QHA24698 Bat CoV Scotophilus kuhlii 512r
APH81308 Porcine epidemic diarrhea virus
A0A1L7HIW4 Lucheng Rn rat CoV
A0A1X9JJV7 Apodemus chevrieri AcCoV-JC34
P36696 Canine CoV strain Insavc-1
Q52PA5 Feline CoV strain FIPV WSU-79/1146
D9J205 Mink CoV strain WD1133
YP_009513022 Porcine CoV HKU15
YP_005352847 Sparrow CoV HKU17
YP_002308480 Bulbul CoV HKU11-934
YP_002308498 Thrush CoV HKU12-600
YP_005352839 White-eye CoV HKU16
YP_002308507 Munia CoV HKU13-3514
YP_005352855 Magpie-robin CoV HKU18
YP_005352882 Common moorhen CoV HKU21
YP_005352864 Night heron CoV HKU19
YP_005352872 Wigeon CoV HKU20
Q14EA8 Human CoV HKU1 isolate N2
Q5MQC8 Human CoV HKU1 isolate N1
Q9IKC8 Rat CoV strain 681
P06591 Murine CoV strain JHM
P0C2R0 Murine CoV strain A59
P29076 Murine CoV strain S
AAC36597 Murine hepatitis virus
A0A0A7UXR5 Rattus CoV HKU24
H9AA36 Rabbit CoV HKU14
AZU96328 Yak CoV
AQT26502 Canine respiratory CoV
AUF40276 Porcine HEV
ACJ35487 Human enteric CoV 4408
ACJ98137 Human CoV OC43
ADX59468 Bat CoV Eidolon helvum
AVP25408 Bat CoV Rousettus HKU9
QDF43841 Bat CoV Rhinolophus affinis GX2018
YP_009273007 Bat CoV Rousettus leschenaulti
QHA24692 Bat CoV Pipistrellus abramus HKU5r
YP_001039967 Bat CoV Pipistrellus HKU5r
A3EXD5 Bat CoV Pipistrellus HKU5
Q0Q4E8 Bat CoV Tylonycteris pachypus
ANA96044 Bat CoV Myotis daubentonii
A3EX99 Bat CoV Tylonycteris HKU4
K9N5R3 Human MERS-related CoV
YP_009361862 Bat CoV Pipistrellus hesperidus
A0A023Y9K8 Bat CoV Vespertilio superans
ASL68947 Bat CoV Hypsugo pulveratus
U5LNK7 Hedgehog CoV Erinaceus amurensis
QCC20719 Hedgehog CoV1
A0A088DKU1 Bat CoV Hipposideros pratti
QID88859 Human SARS-CoV-2 2020_FSS918/AUS
YP_009724392 Human SARS-CoV-2 Wuhan-Hu-1
QHR63302 Bat CoV Rhinolophus affinis RaTG13
PRJNA573298 Pangolin CoV Guangdong
R9QTJ1 Bat CoV Rhinolophus pusillus
A0A166ZL88 Bat CoV Rhinolophus ferrumequinum
D2E1F0 Human SARS coronavirus wtic-MB
AAP73416 Human SARS-CoV ZJ01
P59637 Human SARS-CoV Urbani
AAU04637 Civet SARS-CoV 007/2004
ATO98111 Bat CoV Aselliscus stoliczkanus
A0A0K1Z029 Bat CoV Rhinolophus Ferrumequinum
0.05

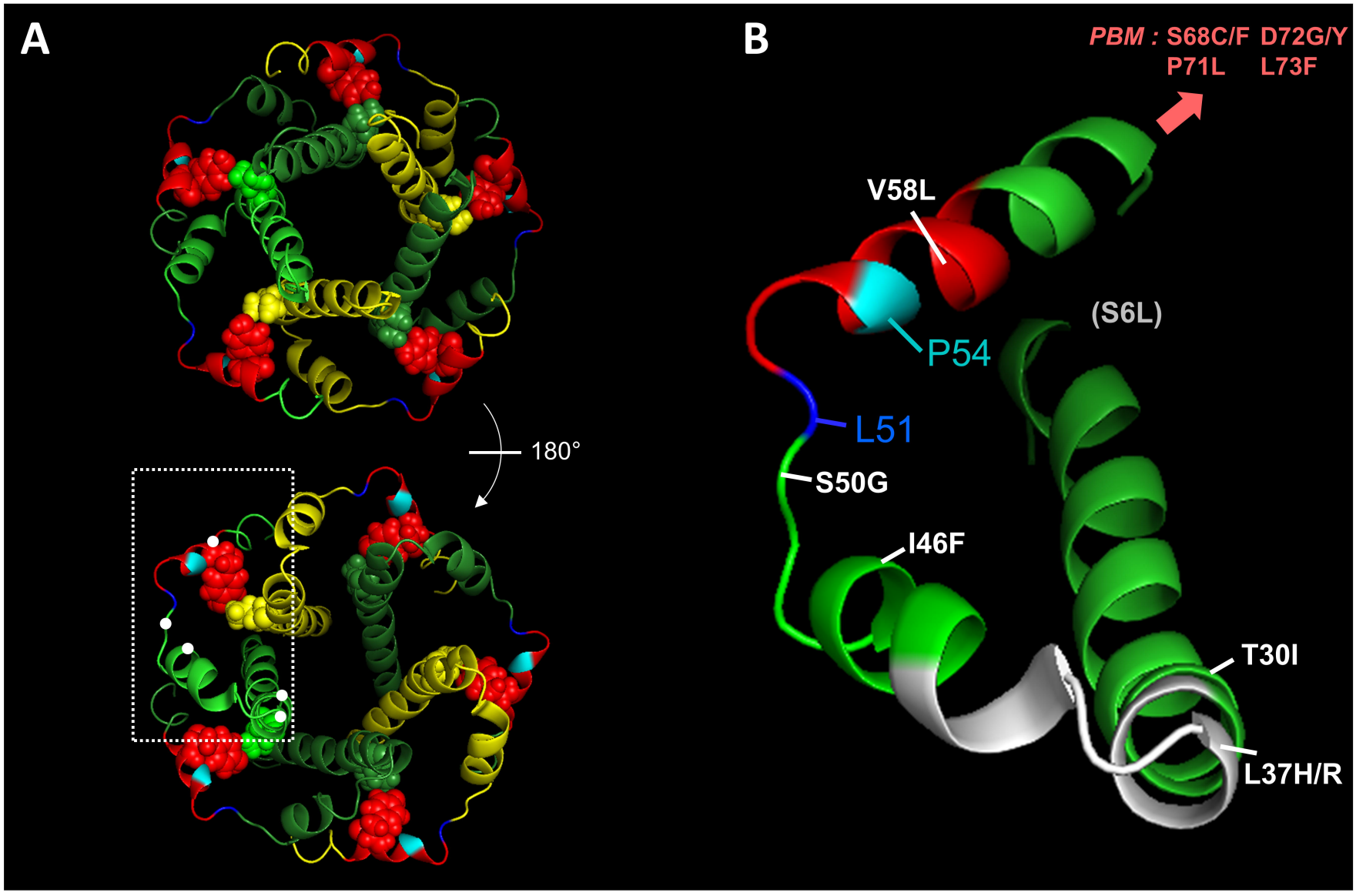

C

```
                                  TRANSMEMBRANE                                  BH3-like      PBM
hSARS-CoV-2 Wuhan-Hu-1            MYSFVSEETGTLIVNSVLLFLAFVVFLLVTLAILTALRLCAYCCNIVNVSLVKPSFYVYSRVKNLNSSRVPDLLV
EPI_ISL_41301526223_26447         MYSFVLEETGTLIVNSVLLFLAFVVFLLVTLAILTALRLCAYCCNIVNVSLVKPSFYVYSRVKNLNSSRVPDLLV
EPI_ISL_41635426213_26437         MYSFVSEETGTLIVNSVLLFLAFVVFLLVILAILTALRLCAYCCNIVNVSLVKPSFYVYSRVKNLNSSRVPDLLV
EPI_ISL_41192926245_26469         MYSFVSEETGTLIVNSVLLFLAFVVFLLVTLAILTAHRLCAYCCNIVNVSLVKPSFYVYSRVKNLNSSRVPDLLV
EPI_ISL_41887425796_26020         MYSFVSEETGTLIVNSVLLFLAFVVFLLVTLAILTARRLCAYCCNIVNVSLVKPSFYVYSRVKNLNSSRVPDLLV
EPI_ISL_41637426195_26419         MYSFVSEETGTLIVNSVLLFLAFVVFLLVTLAILTALRLCAYCCNFVNVSLVKPSFYVYSRVKNLNSSRVPDLLV
EPI_ISL_41830326245_26469         MYSFVSEETGTLIVNSVLLFLAFVVFLLVTLAILTALRLCAYCCNIVNVGLVKPSFYVYSRVKNLNSSRVPDLLV
EPI_ISL_41728526246_26470         MYSFVSEETGTLIVNSVLLFLAFVVFLLVTLAILTALRLCAYCCNIVNVSLVKPSFYLYSRVKNLNSSRVPDLLV
EPI_ISL_41388926245_26469         MYSFVSEETGTLIVNSVLLFLAFVVFLLVTLAILTALRLCAYCCNIVNVSLVKPSFYVYSRVKNLNSCRVPDLLV
EPI_ISL_41641226235_26459         MYSFVSEETGTLIVNSVLLFLAFVVFLLVTLAILTALRLCAYCCNIVNVSLVKPSFYVYSRVKNLNSFRVPDLLV
EPI_ISL_41796926205_26429         MYSFVSEETGTLIVNSVLLFLAFVVFLLVTLAILTALRLCAYCCNIVNVSLVKPSFYVYSRVKNLNSSRVLDLLV
EPI_ISL_41649626245_26469         MYSFVSEETGTLIVNSVLLFLAFVVFLLVTLAILTALRLCAYCCNIVNVSLVKPSFYVYSRVKNLNSSRVPGLLV
EPI_ISL_41468626233_26457         MYSFVSEETGTLIVNSVLLFLAFVVFLLVTLAILTALRLCAYCCNIVNVSLVKPSFYVYSRVKNLNSSRVPYLLV
EPI_ISL_41757126245_26469         MYSFVSEETGTLIVNSVLLFLAFVVFLLVTLAILTALRLCAYCCNIVNVSLVKPSFYVYSRVKNLNSSRVPDFLV
EPI_ISL_41375225865_26065         MYSFVSEETGTLIVNSVLLFLAFVVFLLVTLAI--------YCCNIVNVSLVKPSFYVYSRVKNLNSSRVPDLLV
                consensus          **** ********************** ***        ****:***.*******:********* **  :**
```

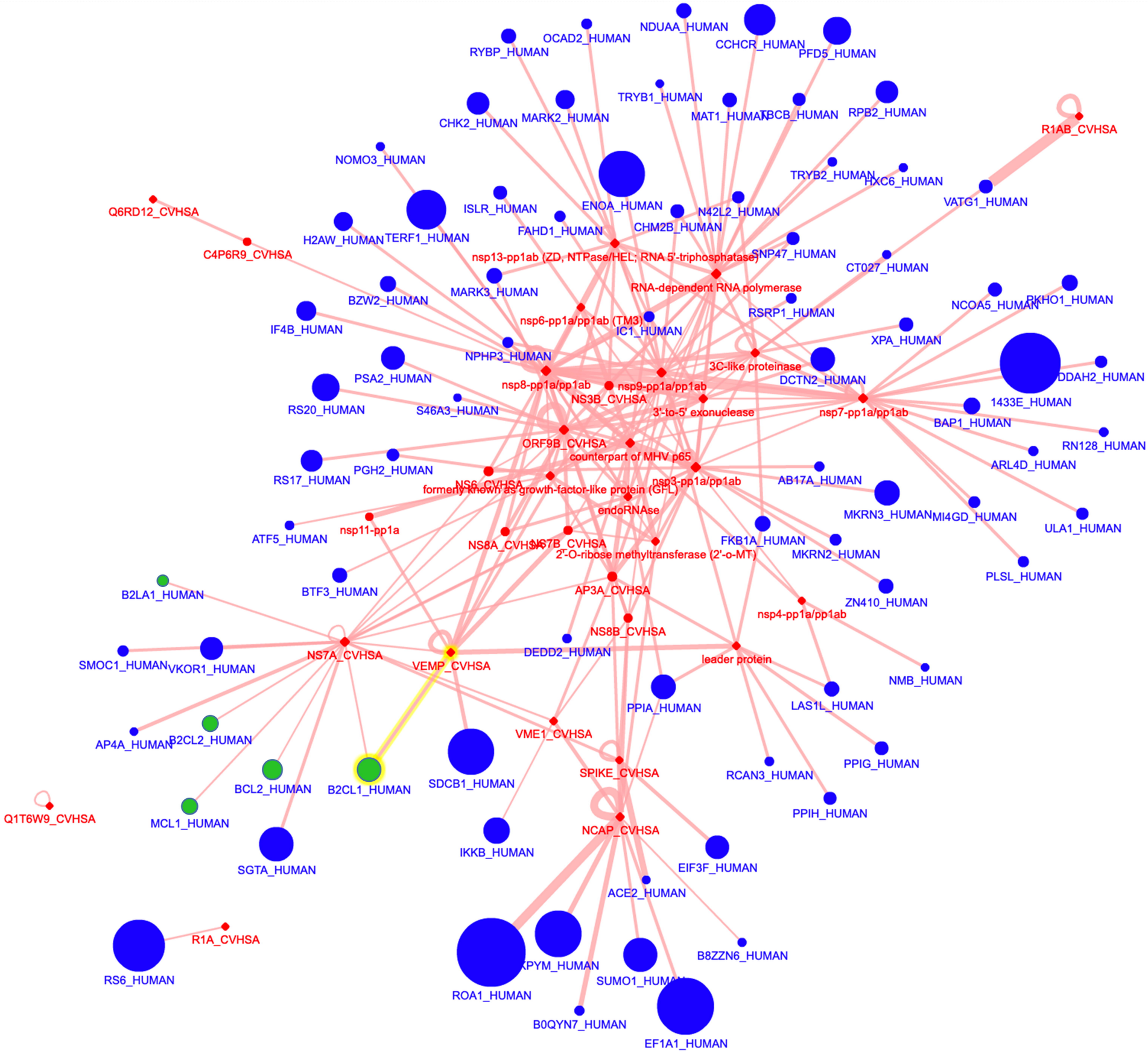
NDUAA_HUMAN
OCAD2_HUMAN
CCHCR_HUMAN
RYBP_HUMAN
PFD5_HUMAN
TRYB1_HUMAN
CHK2_HUMAN
MARK2_HUMAN
MAT1_HUMAN
TBCB_HUMAN
RPB2_HUMAN
R1AB_CVHSA
NOMO3_HUMAN
TRYB2_HUMAN
HXC6_HUMAN
VATG1_HUMAN
Q6RD12_CVHSA
ISLR_HUMAN
ENOA_HUMAN
N42L2_HUMAN
H2AW_HUMAN
TERF1_HUMAN
FAHD1_HUMAN
CHM2B_HUMAN
C4P6R9_CVHSA
nsp13-pp1ab (ZD, NTPase/HEL; RNA 5'-triphosphatase)
SNP47_HUMAN
CT027_HUMAN
MARK3_HUMAN
RNA-dependent RNA polymerase
BZW2_HUMAN
NCOA5_HUMAN
RKHO1_HUMAN
RSRP1_HUMAN
IF4B_HUMAN
nsp6-pp1a/pp1ab (TM3)
IC1_HUMAN
XPA_HUMAN
NPHP3_HUMAN
3C-like proteinase
PSA2_HUMAN
DCTN2_HUMAN
DDAH2_HUMAN
nsp8-pp1a/pp1ab
nsp9-pp1a/pp1ab
RS20_HUMAN
NS3B_CVHSA
S46A3_HUMAN
3'-to-5' exonuclease
nsp7-pp1a/pp1ab
1433E_HUMAN
BAP1_HUMAN
ORF9B_CVHSA
RN128_HUMAN
counterpart of MHV p65
ARL4D_HUMAN
RS17_HUMAN
PGH2_HUMAN
NS6_CVHSA
nsp3-pp1a/pp1ab
AB17A_HUMAN
formerly known as growth-factor-like protein (GFL)
MKRN3_HUMAN
endoRNAse
MI4GD_HUMAN
ULA1_HUMAN
ATF5_HUMAN
nsp11-pp1a
NS8A_CVHSA
NS7B_CVHSA
FKB1A_HUMAN
2'-O-ribose methyltransferase (2'-o-MT)
MKRN2_HUMAN
PLSL_HUMAN
B2LA1_HUMAN
BTF3_HUMAN
AP3A_CVHSA
ZN410_HUMAN
nsp4-pp1a/pp1ab
NS8B_CVHSA
SMOC1_HUMAN
VKOR1_HUMAN
NS7A_CVHSA
VEMP_CVHSA
DEDD2_HUMAN
leader protein
NMB_HUMAN
PPIA_HUMAN
LAS1L_HUMAN
AP4A_HUMAN
B2CL2_HUMAN
VME1_CVHSA
PPIG_HUMAN
SPIKE_CVHSA
RCAN3_HUMAN
BCL2_HUMAN
B2CL1_HUMAN
SDCB1_HUMAN
Q1T6W9_CVHSA
MCL1_HUMAN
PPIH_HUMAN
NCAP_CVHSA
IKKB_HUMAN
SGTA_HUMAN
EIF3F_HUMAN
ACE2_HUMAN
R1A_CVHSA
RS6_HUMAN
B8ZZN6_HUMAN
KPYM_HUMAN
SUMO1_HUMAN
ROA1_HUMAN
B0QYN7_HUMAN
EF1A1_HUMAN

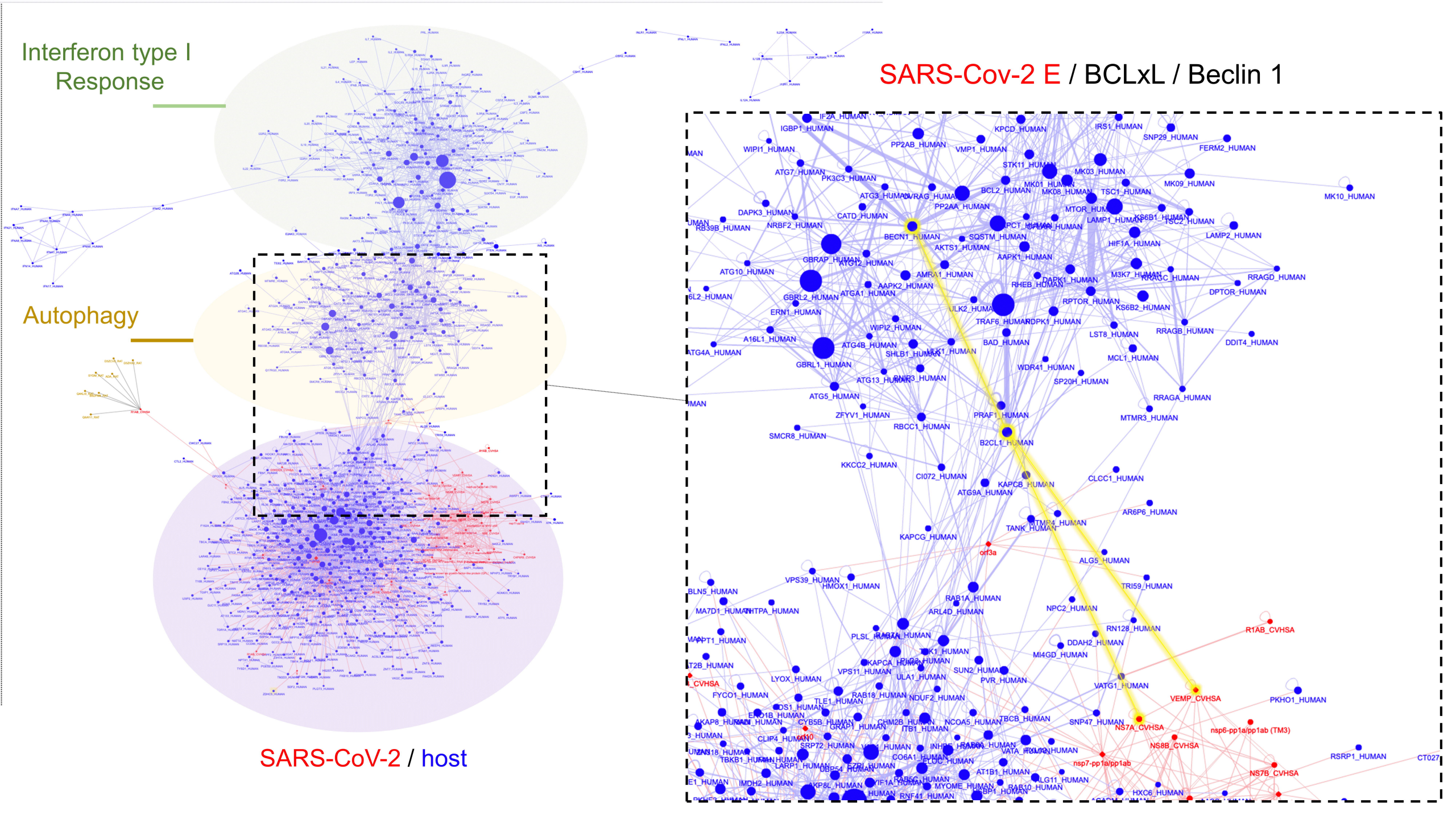
Interferon type I Response
Autophagy
SARS-Cov-2 E / BCLxL / Beclin 1
SARS-CoV-2 / host
IGBP1_HUMAN
WIPI1_HUMAN
ATG7_HUMAN
PK3C3_HUMAN
PP2AB_HUMAN
VMP1_HUMAN
KPCD_HUMAN
IRS1_HUMAN
SNP29_HUMAN
FERM2_HUMAN
STK11_HUMAN
MK03_HUMAN
MK09_HUMAN
MK10_HUMAN
MK01_HUMAN
MK08_HUMAN
TSC1_HUMAN
BCL2_HUMAN
ATG3_HUMAN
PP2AA_HUMAN
DAPK3_HUMAN
CATD_HUMAN
NRBF2_HUMAN
RB39B_HUMAN
BECN1_HUMAN
SQSTM_HUMAN
AKTS1_HUMAN
AAPK1_HUMAN
LAMP1_HUMAN
TSC2_HUMAN
LAMP2_HUMAN
HIF1A_HUMAN
GBRAP_HUMAN
ATG12_HUMAN
ATG10_HUMAN
AMRA1_HUMAN
AAPK2_HUMAN
ATGA1_HUMAN
GBRL2_HUMAN
RHEB_HUMAN
DAPK1_HUMAN
M3K7_HUMAN
RRAGD_HUMAN
DPTOR_HUMAN
RPTOR_HUMAN
KS6B2_HUMAN
ULK2_HUMAN
ERN1_HUMAN
TRAF6_HUMAN
DPK1_HUMAN
WIPI2_HUMAN
A16L1_HUMAN
ATG4B_HUMAN
SHLB1_HUMAN
ULK1_HUMAN
BAD_HUMAN
LST8_HUMAN
RRAGB_HUMAN
DDIT4_HUMAN
ATG4A_HUMAN
GBRL1_HUMAN
MCL1_HUMAN
WDR41_HUMAN
ATG13_HUMAN
BNIP3_HUMAN
SP20H_HUMAN
ATG5_HUMAN
RRAGA_HUMAN
ZFYV1_HUMAN
PRAF1_HUMAN
MTMR3_HUMAN
RBCC1_HUMAN
SMCR8_HUMAN
B2CL1_HUMAN
KKCC2_HUMAN
CI072_HUMAN
KAPCB_HUMAN
CLCC1_HUMAN
ATG9A_HUMAN
AR6P6_HUMAN
TMP4_HUMAN
TANK_HUMAN
KAPCG_HUMAN
orf3a
ALG5_HUMAN
VPS39_HUMAN
HMOX1_HUMAN
TRI59_HUMAN
BLN5_HUMAN
RAB1A_HUMAN
MA7D1_HUMAN
THTPA_HUMAN
ARL4D_HUMAN
NPC2_HUMAN
RN128_HUMAN
R1AB_CVHSA
PPT1_HUMAN
PLSL_HUMAN
DDAH2_HUMAN
MI4GD_HUMAN
T2B_HUMAN
KAPCA_HUMAN
VPS11_HUMAN
SUN2_HUMAN
LYOX_HUMAN
ULA1_HUMAN
PVR_HUMAN
VATG1_HUMAN
FYCO1_HUMAN
RAB18_HUMAN
NDUF2_HUMAN
TLE1_HUMAN
VEMP_CVHSA
PKHO1_HUMAN
ERO1B_HUMAN
CYB5B_HUMAN
CHM2B_HUMAN
NCOA5_HUMAN
TBCB_HUMAN
SNP47_HUMAN
GRAP1_HUMAN
ITB1_HUMAN
NS7A_CVHSA
nsp6-pp1a/pp1ab (TM3)
CLIP4_HUMAN
SRP72_HUMAN
NS8B_CVHSA
TBKB1_HUMAN
CO6A1_HUMAN
LARP1_HUMAN
nsp7-pp1a/pp1ab
RSRP1_HUMAN
AT1B1_HUMAN
NS7B_CVHSA
IMDH2_HUMAN
MYOME_HUMAN
RAB10_HUMAN
HXC6_HUMAN
RNF41_HUMAN